This paper was published in Applied Optics (2011) 50:6039-6048 and is made available as an electronic reprint with the permission of OSA. The paper can be found at the following URL on the OSA website: http://www.opticsinfobase.org/ao/abstract.cfm?uri=ao-50-32-6039. Systematic or multiple reproduction or distribution to multiple locations via electronic or other means is prohibited and is subject to penalties under law.

High precision dynamic multi-interface profilometry with optical coherence tomography

Samuel Lawman, Haida Liang*

School of Science & Technology, Nottingham Trent University, Clifton Lane, Nottingham NG11 8NS, UK

**Corresponding author: haida.liang@ntu.ac.uk*

Optical coherence tomography (OCT) has mostly been used for high speed volume imaging but its profilometry potentials have not been fully exploited. This paper demonstrates high precision (as good as ~50nm) multi-interface profilometry using a Fourier domain OCT system without special anti-vibration devices. The precision is up to two orders of magnitudes better than the depth resolution of the OCT. Detailed analysis of the precision achieved for different surfaces is presented. The multi-interface profiles are obtained as a by-product of the tomography data. OCT has advantage in speed and sensitivity at detecting rough and internal interfaces compared to conventional optical profilometry. An application of the technique to the dynamic monitoring of varnish drying on paint-like substrates is demonstrated, which provides a better understanding of the

formation of surface roughness. The technique has potential benefits in the field of art conservation, coatings technology and soft matter physics.

OCIS codes: 110.4500 (Optical Coherence Tomography); 120.3180 (Interferometry); 120.6660 (Surface measurements, roughness).

1. Introduction

Optical Coherence Tomography (OCT) is an optical interferometric technique that has been developed in the last 20 years with the aim of providing fast, high resolution and high contrast *in vivo* optical sectioning of the eye and other biological tissues [1,2,3,4]. OCT has found a wide variety of applications in biomedicine and its use has been expanded into non-medical fields [5] including art conservation and archaeology [6,7]. There are two modalities of OCT: Time Domain (TD) and Fourier Domain (FD) [8]. In TD OCT, depth ranging is achieved through scanning the mirror in the reference arm of the interferometer. In FD OCT, the reference mirror is fixed and the interference signal is recorded as a function of wavelength using either a spectrometer or a swept source. The spectrum is then Fourier transformed to give the final image.

Profilometry is the measurement of surface profiles and the acquisition of statistical values of roughness from these profiles [9]. It is an important technique in engineering and optics to quantify the quality of surfaces [10]. There are two common classes of profilometry methods: 1) contact mechanical profilometry and 2) a wide variety of non-contact optical techniques including confocal microscopy and interferometry. For smooth continuous surfaces, such as lenses, phase shifting interferometer [11] is a powerful tool that deduces the surface profile from the phase of the interference pattern. However, for surfaces with steep slopes, discontinuities or

significant roughness, White Light Interferometry (WLI) [12,13] is better at recording the position of the surface, by measuring the centre of the coherence envelope of the returned signal rather than small relative phase differences.

Both OCT and WLI are broadband Michelson interferometers but with different emphasis. OCT is optimized for high signal-to-noise, rapid tomography with large depth range and WLI is often optimized for high precision profilometry of relatively smooth material. Commonly in WLI, a time domain setup is used with a broad spectral band thermal source. In contrast, OCT makes use of light sources, such as superluminescent diodes (SLD), with a high intensity and a near Gaussian spectrum to obtain rapid high signal-to-noise images. The Fourier domain method is common in OCT due to benefits in speed and signal-to-noise ratio of measurements, whereas FD modality in WLI profilometry is relatively rare [14,15]. In WLI profilometry, the best possible precision is usually quoted in the nanometers [16], whereas in OCT typical precisions are quoted in microns [17].

Since WLI based optical profilometry and OCT both use broadband Michelson interferometry, they should in principle yield similar precision in profilometry. However, as OCT was developed for *in vivo* tomography, its application in precision profilometry has not been well developed. The axial resolution of both OCT and WLI are inversely proportional to the source bandwidth for the same central wavelength. While WLI use thermal sources which have about 3 times the bandwidth of a SLD typically used in OCT, the precision in profilometry commonly quoted for WLI is 3 to 4 orders of magnitude better than that of OCT. In reality, the position of the surface or the peak of the axial PSF can be determined to much higher accuracy than the depth resolution. The factors that determine the position accuracy are the signal-to-noise ratio of the intensity peak, vibrational stability of the instrument, accuracy of the peak finding

algorithm and the nature of the surface roughness. By using high intensity sources such as SLDs, OCT has much higher sensitivity than the common WLI based optical profilometers using thermal sources. This gives OCT the advantage of profilometry on multiple faint interfaces rather than just the top surface.

In this paper, multi-interface OCT profilometry is applied to the dynamic monitoring of varnish coatings on rough substrates. Varnish coatings are used on paintings to serve two purposes: 1) as a protective layer for the paint and 2) as an optical element that changes the appearance of the painting. Raw paint surfaces are generally matte and hence diffusely scatter white light. The observer sees both the diffuse surface scattered white light and the volume scattered colored light from the paint. Since the varnish coating applied on top gives a smoother surface than the paint surface, the light reflected from the varnish surface is dominated more by specular than diffuse reflections. The increased gloss results in an increase in the apparent chroma of the paint when viewed away from the specular direction.

It has long been recognized that different types of varnish give different optical appearances to a painting. Berns and de la Rie [18] showed that it was the ability of a varnish to produce a smooth surface when applied to a rough paint surface, rather than differences in refractive index, that determined their different effect on the optical appearance of a painting. Subsequent measurements of the surface roughness of two varnish resins, AYAT (a high weight PVAe polymer) and Regalrez (a low molecular mass oligomer) when applied to substrates of different roughness, were shown to be dependent on the roughness of the substrate and the type of varnish [19]. However, the use of mechanical profilometry and later laser scanning confocal microscopy [20] only allowed the measurement of the top surface, and hence no direct correlation of the varnish surface profile to the substrate beneath could be shown. Preliminary

OCT monitoring of a Paraloid B72 varnish drying on a regular rough surface showed that the varnish follows the roughness of the substrate as it dried [21]. Subsequently, OCT imaging of a Ketone varnish and a Paraloid B67 varnish on a painting showed directly that the low molecular weight Ketone varnish was better at leveling the surface roughness of the painting [6]. However, neither study showed high precision quantitative profiles of the interfaces. Multi-interface profilometry with OCT allows the simultaneous measurement of both the top surface and the substrate profile beneath making it possible to directly correlate the two interface profiles. Multi-interface OCT profiometry is used in this paper to measure dynamic evolution of the surface profile and the cross-correlation between the surface and substrate profiles for two very different drying varnish coatings. The dynamic development of the surface profile is modeled numerically using the differential lubrication approximation to the Navier-Stokes equation [22,23]. The modeled and experimental surface profiles are compared directly to better understand the relationship between the material properties of a varnish and the formation of the surface roughness of varnish on a rough paint-like substrate..

Previously the authors presented preliminary results on the use of OCT for multiple interface profilometry in a conference proceeding [24]. The evaluation of the accuracy on a standard flat surface gave a standard deviation of 55nm for the positional accuracy. The ranging accuracy was examined using a stepped surface and found to be consistent with the positional accuracy. This study also examined the potential of the technique on random rough surfaces. Important results from the preliminary study will be recapitulated and expanded on in this paper along with new results on applications of the technique. The paper is organized into the following sections. Section 2 describes the detailed characteristics of the OCT used, the necessary instrumental corrections and the processing method for OCT profilometry. Section 3

examines the precision of OCT surface profilometry for smooth surfaces, sinusoidal surfaces and random rough surfaces. Section 4 examines the capabilities of OCT profilometry for multiple interfaces of layered systems, including the determination of the refractive index of the top layer for the correction of optical distortions necessary for the recovery of the internal interface profiles. Section 5 shows an application of OCT multi-interface profilometry on the dynamic monitoring of the drying of two different types of varnish on a paint-like substrate, as well as a model for the surface roughness formation as a varnish dries. Section 6 gives the conclusions.

2. Instrument and methods

The results in this paper are obtained with a Fourier domain Thorlabs SROCT which consists of a Michelson interferometer, a SLD light source (central wavelength of 930nm and bandwidth of 100nm) and a spectrometer. The interferometer and the one axis lateral scanning mechanism are enclosed in a handheld probe. The spectrometer and light source are located in a separate base unit connected to the handheld probe by an optical fiber. The axial resolution of the system is 6.5μm in air, the transverse resolution is 9μm and the maximum depth range is 1.6mm. A Hann window function was used to taper the spectrum. For the following measurements, the handheld probe is secured to a 3-axes motorized micrometer stage.

The optics in the OCT system was telecentric leading to no noticeable “fan beam” distortions [17]. However, the line of equal path length in the 2D image is not flat over the field of view. This is visible in the curvature of the OCT image, and hence the measurement of the surface profile of a standard flat surface can be used to correct any measured surface profile by subtraction. This method was essential for all measurements of profiles greater than 1mm in lateral range.

The axial sample response function of an interface is a δ-function because of the refractive index discontinuity. The measured axial intensity profile is the convolution of the sample response function with the axial point spread function (PSF) of the instrument. Figure 1a shows an example of a Gaussian fit to an interface in tomography data of an OCT image. The fitting of a Gaussian function to this depth intensity profile allows the position of the surface to be found with accuracy much higher than the axial resolution of the system.

Lateral profiles other than the top surface profile are distorted by the optical path length (group refractive index) and refraction (phase refractive index) of the material above. In this paper, group refractive index is assumed to equal phase refractive index. The real position of the second interface is corrected by a 2D Snell's law correction [25]. In this study no data was taken in the other lateral dimension to enable a 3D refraction correction [26].

3. Performance of OCT surface profilometry

3.1 Smooth Surface Performance

The main source of error in the measurement of a smooth surface profile was found to be vibration in the system which can be reduced by averaging a number of frames. To quantify the accuracy of the measurement, a standard flat surface was measured. Figure 1b shows the decrease in the standard deviation of the surface profile with increasing number of averaged frames. The standard deviation of the surface measurement after averaging is shown to level out at 55nm after 20 averages. The value quoted is typical of a measurement during the day on a lab bench without the use of special anti-vibration devices. Recently, Prykäri et al. [27] used an ultra-high resolution (submicron axial resolution) TD OCT to measure the topography of glossy paper. By measuring the highest intensity point on a highly sampled interferogram, a 1σ□

accuracy of 60nm for the surface profile was quoted, which we have shown to be possible with a much lower resolution OCT without the need to develop expensive ultra-high resolution OCT.

Verification of the positional reliability of the method was carried out with a standard step surface of 9.932μm in step height. This is a standard surface that is used to calibrate commercial optical profilometers (Veeco). The surface profile and step height is extracted from the mean of 60 OCT images. The step height was measured at 6 separate locations on the surface with the OCT which gave a mean of 9.94 ± 0.04μm consistent with the quoted reference value. The uncertainty in this measurement is similar in magnitude to that of the standard flat surface.

3.2 Sinusoidal surface performance

Due to the coherent nature of OCT, speckle [28] is a major source of error when measuring profiles of rough/matte surfaces. The simplest case of such a surface is a sinusoid, which can be regarded as a regular rough surface with only one component of spatial frequency.

It is well known that commercial WLI profilometers are susceptible to artifacts when measuring sinusoidal surfaces [16]. To compare the performance of OCT profilometry against a commercial WLI profilometer (Veeco inc. Wyko NT1100), measurements were taken of a sinusoidal surface with peak-to-peak amplitude of 1.5μm and period of 50μm. Figure 2a shows an OCT image of this surface. To measure quantitatively the distortions of each measurement, the expected sinusoid shape was fitted to the profiles. The measured profiles and fits are shown for measurements with the SROCT (Fig. 2b) and the Veeco WLI (Fig 2c). The *rms* of the residual from the fit for the SROCT is 0.27μm and for the Veeco WLI is 0.26μm, showing that the errors are similar.

3.3 Random rough surface performance

The commercial WLI, with its thermal light source, was unable to see the random rough surfaces used in this study. The sensitivity of OCT makes it easy to measure these optically matte surfaces [24,29]. Amaral et al [29] found that with a single profile measurement of random rough surfaces with small *rms* roughness their OCT method significantly overestimated the true roughness. Here we show that this is due to speckle error dominating the measured surface profile.

The SROCT was used to measure the surface profile at four different axial distances from the sample (100μm intervals), each with an average of 60 frames. In the absence of speckle, the measured profiles should be identical within measurement errors of 55nm as found in the measurement of the standard flat surface. By assuming Gaussian distribution of surface position and measurement errors, the effect of speckle and surface roughness can be calculated from the difference between two profiles measured from different working distances from the sample. If the effect of speckle in the data of each measured profile is completely de-correlated, the *rms* difference between two axially shifted measurements of the same profile, σ_D, is then given by $\sigma_D{}^2 = 2\sigma_S{}^2 + 2\sigma_V{}^2$, where σ_S is the speckle noise and σ_V is the vibration noise. The value of the measured *rms* roughness σ_M of a single profile is then given by $\sigma_M^2 = \sigma_T^2 + \sigma_D^2/2$, where σ_T is the true surface roughness. The shifting of the axial measurements is also moving the surface in relation to the position of focus of the system. While speckles become more de-correlated with a changing spot size, measurement accuracy for the surface will also decrease with distance from the focus. To reach a compromise, the axial range of measurements was kept within a couple hundred micron range of the focus. Other potential sources of error include alignment errors causing the profiles to be different when measured at different distance from the probe, and hence over-estimating the speckle noise and under-estimating the true roughness. If the speckles

are not fully de-correlated, then this method is likely to under-estimate the speckle noise and over-estimate the true roughness.

Performance was evaluated on two random rough surfaces. The first of these has a *rms* roughness of 0.67μm measured with a mechanical profilometer with a stylus radius of 2μm in a previous study [19]. For this surface, the error due to speckle was found to be 0.90 ± 0.10μm and the *rms* surface roughness was measured to be 0.76 ± 0.17μm consistent with the roughness measured with the mechanical profilometer. The error in profile measurements due to speckle is larger than the surface roughness for this sample. Therefore it would not be possible to recover the surface profile from a single measurement, even though an accurate estimate for the *rms* roughness is possible.

A second rough surface with *rms* roughness approximately ten times larger was again measured with the SROCT at different axial positions. The *rms* surface roughness was measured to be 9.91 ± 0.18μm and error due to speckle was 3.10 ± 0.44μm. In this case, even though the error due to speckle was very high, it was significantly less than the profile *rms* roughness. The speckle noise also gives an indication of the roughness on scales smaller than the lateral resolution. In the above two cases, the speckle noise increases with the larger scale surface roughness.

This simple statistical method for measuring random rough surfaces gives not only the *rms* roughness but also an indication of the uncertainty in the measured surface profile due to speckle.

4. Multiple interface profilometry

OCT is designed for rapid *in vivo* tomographic imaging which ensures high sensitivity. This high sensitivity means that weak reflections from internal interfaces are visible in the image. The

OCT profilometry technique can be extended to these internal interfaces to perform multiple interface profilometry.

4.1 Refractive index measurement

In order to correct for optical path length and refraction distortions, the refractive index of the material needs to be known. To determine the refractive index of the varnish to be used in Section 4.2, a droplet of the varnish solution (Regalrez resin dissolved in white spirit) is placed upon a flat microscope slide. An OCT measurement is carried out through the centre of the droplet so that the angle of incidence is normal to the microscope slide and the droplet surface (Fig 3a). Due to the unequal instrumental optical path length across the field of view (Sec. 2), the microscope slide appears to be tilted in the OCT image. The following positions are found with high precision (Fig 3b): 1) the position of the air/droplet interface (z_1), 2) the apparent position of the droplet/microscope slide interface beneath (z_2), and 3) the real position of the droplet/microscope slide interface obtained by interpolation from the air/microscope slide interface on each side of the droplet (z_3). The refractive index is measured by taking the ratio between the optical and real thicknesses of the droplet: $n = \frac{z_1 - z_2}{z_1 - z_3}$. The refractive index of the white spirit (n=1.41-1.44) is lower than the refractive index of the Regalrez resin (n=1.52) [18]. Figure 3c shows that as the concentration increases by evaporation of white spirit, the refractive index of the droplet increases.

A number of papers have been published previously with techniques similar to the above for measuring refractive indices with OCT [30-32]. An increase in position accuracy of determining the interfaces enables better accuracy in refractive index measurements. While the previous studies quoted refractive index accuracies similar to this study, the measurements were

obtained from much thicker samples of ~1mm compared with 20 to 150μm in the current study. Given the method of refractive index determination, measurements on thick samples will in general give better accuracy than those on thinner samples. For example, in the refractive index measurements of ~1mm thick fused silica by Wang et al [31] using a similar method, the thickness accuracy was 5μm, which gave a refractive index error of 0.005. If this had been carried out on a 29μm thick sample, the refractive index error would have been 0.1. Whereas in the refractive index measurements of the drying droplets above, the median 1σ refractive index error was 0.003 for a median thickness of 29μm. The much improved position accuracy in the current study enables a potential 30 times improvement in the accuracy of refractive index measurement.

4.2 Measurement of Rough Internal Interfaces

The application of multi-interface OCT profilometry to a drying varnish coating on a rough glass substrate (13μm *rms* roughness), allows the simultaneous measurement of the smooth varnish surface profile and the substrate profile. To determine the accuracy of recovering the rough substrate profile after correcting for both the optical thickness and refractive effects due to Snell's law, the coarse rough surface was initially measured with the SROCT over a range of 10mm. Without moving the instrument or the substrate, a varnish solution of Regalrez 1094 dissolved in white spirit at a ratio of 1g of resin to 1ml of solvent, was applied by a pipette from the side and left to spread, so that approximately half the surface in the OCT image was covered with the solution.

Due to the massive difference in the intensity of the Fresnel reflection from the air/varnish interface and varnish/glass interface, care needs to be taken in finding the second interface to distinguish it from harmonic and ringing artifacts. In addition, a post processing

algorithm for the removal of remaining ringing artifacts and anomalous points was devised and implemented in MATLAB. The 2D Snell's law refractive index correction was then carried out to find the correct second interface. A final result showing the rough substrate profile before and after the application of varnish and the difference between the two are shown in Fig. 4. The outliers in the difference graph are incorrect identifications of the interface by the automatic routine due to the presence of image artifacts.

To determine the effect of refractive index in the correction of second interface measurements, each measured varnish/substrate profile was corrected for a range of refractive indices. The *rms* of the difference between the measured glass substrate profile before application of the varnish and those of the same substrate profile recovered from below the varnish using various refractive index values are shown in Fig. 5. A minimum occurs at the refractive index value corresponding to that measured in Section 4.1. The minimum *rms* difference approaches the measured speckle error of the substrate surface. Figure 5 shows that for this coarse substrate, a refractive index accuracy of 0.05 is needed to ensure that the error due to refractive index correction is not significant compared to speckle error.

5. Dynamic monitoring of surface roughness formation of a drying varnish

The final roughness of varnish has previously been shown to be dependent on the roughness of the substrate and the type of varnish resin [19]. However, the direct dynamic correlation of the surface profile with the substrate profile had not been studied previously. OCT multi-interface profilometry can measure the correlation of the varnish and substrate profiles directly and dynamically during the drying process. The lubrication approximation to the Navier-Stokes

equation can be used to model the formation of the varnish surface profile to compare with the measured time evolution of the varnish surface profiles.

As a varnish coating dries by the evaporation of solvent, its volume decreases. As it shrinks, the surface profile will take the shape of the substrate beneath. This development of surface roughness increases surface area and hence total surface energy. Surface tension acts against this increase in surface energy by driving a leveling flow to smooth the varnish. This flow can be modeled by the differential of the surface profile Φ(x) given by

$$\Delta\Phi(x) = \Delta h(x) = \left\{ \frac{1}{3} \frac{\gamma}{\eta(C(x))} \frac{\Delta}{\Delta x} \left[\left(\frac{\Delta^3 \Phi(x)}{\Delta x^3} \right) h(x)^3 \right] + E(C(x)) \right\} \Delta t \qquad (1)$$

where γ is the surface tension, η is the viscosity of the varnish, x is lateral position, h is the varnish thickness, C is concentration, E is the change in thickness as a result of evaporation and Δt is the time interval [22,23]. For the model, the surface tension is kept as a constant while the viscosity is determined empirically as a function of concentration from experimental rheology data. The concentration at each lateral position is determined from the initial concentration and the evaporation function as time evolves. The evaporation function is determined empirically from gravimetric measurements of the drying varnish sample. The initial state of the varnish is assumed to be a perfectly flat film of uniform initial concentration.

The dynamic drying of two very different varnish solutions was monitored using the OCT. An AYAT varnish made up of 3g of the polymer AYAT mixed in 11ml of toluene (viscosity of 0.456 Pa.s) was applied to a coarse glass substrate with a bird type applicator (225μm gap or varnish thickness of 145μm). The drying was measured with the SROCT at intervals of approximately 10 seconds. Figure 6 shows the experimental and modeled time evolution of the varnish surface profile during the drying of the varnish with the simultaneously

measured substrate profile. Apart from a time delay between the experimental and theoretical starting point expected from the time lapse between the application of varnish and starting the OCT measurements, these direct comparisons of the profiles show that the model produces a close match to the measured surface profile. To compare with the AYAT results, a Regalrez in toluene varnish was applied to a similar rough substrate. It was applied at a concentration of 1g of Regalrez in 1ml of toluene (viscosity of 0.011 Pa.s) with an applicator gap of 100 μm (or varnish thickness of 70μm), to give approximately the same dry varnish thickness as in the AYAT measurement.

The simplest parameter to describe roughness is the *rms* surface roughness. However, this does not contain important spatial information about the surface. Alternatively, Power Spectral Density (PSD) shows the amplitude of roughness as a function of spatial frequency. Figure 7 shows the PSDs of both the modeled and measured final surface profile of the AYAT and Regalrez varnish coatings along with the mean PSD of the two substrate profiles. As has been shown in previous studies [19], both varnishes reduce the higher spatial frequency components of substrate roughness, with Regalrez reducing it more over a larger spatial frequency range than AYAT. The huge difference in viscosity as a function of concentration is the main reason for the difference in the leveling of the two varnishes. AYAT is orders of magnitude more viscous than Regalrez at any concentration. Figure 7 shows that the apparent deviation of the modeled PSD from the measured ones for Regalrez varnish at high frequencies is due to vibration noise.

To compare the development of roughness in different spatial regimes, a high pass and a low pass filter were used to separate the high (above 1 mm^{-1}) and low spatial frequencies (below 1 mm^{-1}) of the interface profiles. Figure 8a,b show the experimental and modeled development of the *rms* surface roughness in different spatial frequency windows as a function of time for

each varnish. For the AYAT varnish, the roughness develops in both spatial regimes during the 15 minutes of drying. There is a time displacement between the model and experimental results which is partly due to the time delay between the application of varnish and the start of OCT monitoring. Both the model and the experimental results show the low frequency surface roughness developing before the high spatial frequency roughness. The sharp glitch in the roughness measurement is due to a sudden vibration (Fig. 8a). For the Regalrez varnish, the measured roughness in the low spatial frequencies rapidly developed during or immediately after application but before OCT monitoring started. The initial glitch in the low frequency roughness of Regalrez varnish is most likely to be due to the varnish settling since it is still liquid at that point (Fig. 8b). Both the measured and modeled late time roughness for Regalrez varnish is significantly less than that of AYAT varnish on all spatial scales. The model prediction for Regalrez significantly underestimates the surface roughness in the low spatial frequencies. This may be the result of Bénard-Marangoni convection [33] which has not been taken into account by the model.

A key aspect of multi-interface profilometry is the direct measurement of the cross-correlation between the surface and substrate profiles. The time evolution of the experimental and modeled cross-correlation coefficients taking into account the effects of vibration for various spatial frequency windows are shown in Fig. 8c,d, where for AYAT these follow closely the corresponding time evolution in the *rms* roughness. Between 6-7 minutes, there is a rapid increase in correlated roughness which also corresponds to a change in the rate of decrease in thickness as a function of time (Fig. 8e). The trends of the experimental and modeled results show reasonable agreement. Throughout the drying process, the low spatial frequency component show stronger cross-correlation than the high spatial frequency components. For

Regalrez varnish, the model predicts higher correlation than the measured values in the low spatial frequencies. The Regalrez and AYAT coatings were also applied to smooth glass substrates where the Regalrez varnish still developed the low spatial frequency roughness while the AYAT did not. The development of the low spatial frequency roughness of the Regalrez varnish was independent of the substrate. The cause of this roughness is likely to be Marangoni effect [33]. The reduced mobility of AYAT compared to Regalrez may be the reason that it is not susceptible to the same effects.

Comparison of the modeled and measured thickness of the coatings (Fig 8e for AYAT and Fig 8f for Regalrez) enables the accuracy of the evaporation parameters of the model to be assessed. There are some differences between the modeled and experimental results. The final measured thicknesses of the coatings are greater than the model predictions. This is partly due to the model assumption of volume conservation in a resin/solvent mixture which is not always true in reality and would then lead to the over-estimation of the change in volume with evaporation. Future refinements of the model could include a more realistic concentration versus varnish thickness relation as well as exploring different extrapolations of the concentration versus viscosity relation in late times when it is not possible to measure the viscosity directly.

Multi-interface profilometry with OCT is a powerful technique for measuring the drying of varnishes. It has the ability to measure film thickness and how the surface profile of the varnish develops in relation to the substrate profile during the drying process. The rapid dynamic measurements allow detailed studies of the drying process. This technique is being used as part of a study of the physics of drying varnishes to quantify how the material properties of varnish such as surface tension, viscosity and evaporation rate affects the formation of the varnish

surface, and hence provide a recipe for varnish mixtures that can produce the desired optical appearance.

6. Conclusions

It has been shown that surface profiles can be extracted from OCT data with a precision two orders of magnitude higher than the axial resolution of the instrument when a Gaussian function is fitted to the axial PSF. An *rms* precision of 55nm was achieved for a smooth surface using an OCT with an axial resolution of 6.5μm. The interface profiles can be extracted by post-processing of previously collected data without any special measurement procedure. With the SROCT used in this study it is also possible to measure the *rms* roughness value of surfaces even when the error due to speckle is higher than this value.

Multi-interface profilometry is ultimately limited by the resolution of the system when dealing with layers thinner than the depth resolution. While improving the resolution of OCT may improve the accuracy in OCT profilometry, orders of magnitude improvements can already be made with a simple post-processing method described in this paper.

The high sensitivity of OCT allows not only the top surface but also the faint internal interfaces to be measured with high accuracy. OCT multi-interface profilometry has the potential to be an invaluable tool for the study of the relationship between material properties of a varnish and the formation of surface roughness which in turn influences its optical properties. The surface roughness of a varnish coating and the profile of the substrate beneath can be measured simultaneously, allowing direct comparison to be made of the surface profile of the varnish and the varnish/substrate interface.

OCT profilometry has the advantage of rapid monitoring compared with conventional profilometry techniques, which is important for applications that require dynamic monitoring.

An example of such an application has been demonstrated through the dynamic monitoring of the drying process of a varnish solution on a paint-like interface which has both practical applications in art conservation and importance in theoretical understanding in soft matter physics. A simple lubrication approximation to the Navier-Stokes equation was used to model the dynamic formation of the varnish surfaces for two very different varnish solutions. The modeled surface profiles were compared directly with the measured surface profile during the drying process, which enables refinement of the model. The parameters of the model can be varied to determine what combination of properties of synthetic varnish solutions can give the desired surface state similar to those given by varnishes based on natural resins, since these are thought to give paintings the preferred optical appearance.

Acknowledgements

This work was supported by a UK Engineering and Physical Sciences Research Council CASE award, the Leverhulme Trust and the National Gallery. We would like to thank Rene de la Rie and Marika Spring for providing us with samples and for useful discussions about varnishes used in conservation, and Robert Huber for useful discussions.

References

1. D. Huang, E. A. Swanson, C. P. Lin, J. S. Schuman, W. G. Stinson, W. Chang, M. R. Hee, T. Flotte, K. Gregory, C. A. Puliafito, J. G. Fujimoto, “Optical coherence tomography,” Science, 254, 1178-1181 (1991).
2. A. F. Fercher, W. Drexler, C. K. Hitzenberger and T. Lasser, “Optical coherence tomography – principles and applications”, Rep. Prog. Phys., 66, 239-303 (2003).

3. P. H. Tomlins and R. K. Wang, “Theory, developments and applications of optical coherence tomography”, J. Phys. D: Appl. Phys, 38, 2519-2535 (2005).
4. W. Drexler and J. G. Fujimoto, *Optical Coherence Tomography Technology and Applications* (Springer, 2008).
5. D. Stifter, “Beyond biomedicine: a review of alternative applications and developments for optical coherence tomography”, Appl. Phys. B, 88, 337-357 (2007).
6. P. Targowski, M. Góra and M Wojtkowski, “Optical Coherence Tomography for Artwork Diagnostics”, Laser Chemistry, doi:10.1155/2006/35373 (2006)
7. H. Liang, B. Peric, M. Hughes, A. G. Podoleanu, M. Spring, and S. Roehrs, “Optical Coherence Tomography in archaeological and conservation science - a new emerging field”, Proc. SPIE 7139, 713915 (2008).
8. A. F. Fercher, C. K. Hizenberger, G. Kamp and S. Y. El-Zaiat, “Measurement of intraocular distances by backscattering spectral interferometry”, Optics Communications, 117, 43-48 (1995).
9. K. J. Stout and L. Blunt, *Three Dimensional Surface Topography* (Penton Press, 2000).
10. J. M. Bennett, and L. Mattson, *Introduction to surface roughness and scattering* (Optical society of America, Washington, 1989).
11. H. Schreiber and John H. Bruning, “Phase Shifting Interferometry”, in *Optical Shop Testing*, D. Malacara, ed. Wiley-Interscience (2007), pp. 547-666.
12. B. S. Lee and T. C. Strand, 1990, “Profilometry with a coherence scanning microscope”, Appl. Opt. 29, 3784-3788 (1990).
13. T. Dresel, G. Häusler, and H. Venzke, “Three-dimensional sensing of rough surfaces by coherence radar“, Applied Optics, 31 (7), 919–915 (1992).

14. T. Endo, Y. Yasuno, S. Makita, M. Itoh, and T. Yatagai, “Profilometry with line-field Fourier-domain interferometry”, Optics Express, 13 (3), 695–701 (2005).
15. D. Renlon, M. Jacquot, I. Verrier, G. Brun, and C. Veillas, “Broadband supercontinuum interferometer for high-resolution profilometry”, Optics Express, 14 (1), 128–137 (2005).
16. F. Gao, R. K. Leach, J. Petzing, and J. M. Coupland, “Surface measurement errors using commercial scanning white light interferometers”, Meas. Sci. Technol., 19, 015303 (2008).
17. S. Ortiz, D. Siedlecki, L. Remon and S. Marcos, “Optical coherence tomography for quantative surface topography”, Applied Optics, 48 (35), 6708-6715 (2009).
18. R. S. Berns and E. R. de la Rie, “The effect of Refractive Index of a Varnish on the Appearance of Oil Paintings”, Studies in Conservation, 48 (4), 73-83 (2003).
19. M. Elias, E. R. da la Rie, J. K. Delaney, E. Charron and K. M. Morales, “Modification of the surface state of rough substrates by two different varnishes and influence on the reflected light”, Optics Communications, 266, 586-591 (2006).
20. J. K. Delaney, E. R. de la Rie, M. Elias, L. P. Sung and K. M. Morales, “The role of varnishes in modifying light reflection from rough surfaces”, Studies in conservation, 53, 170-186 (2008).
21. H. Liang, M. G. Cid, R. Cucu, G. Dobre, B. Kudimov, J. Pedro, D. Saunders, J. Cupitt, and A. Podoleanu, "Optical coherence tomography: a non-invasive technique applied to conservation of paintings", Proc. SPIE 5857, 261-269 (2005).
22. L. E. Stillwagon and R. G. Larson, “Fundamentals of topographic substrate leveling”, J. Appl. Phys., 63 (11), 5251-5258 (1988).

23. M. D. Bullwinkel, J. Gu and G. A. Campbell, “The effect of drying rate on film leveling over an uneven substrate surface”, in *ANTEC ’97 - plastics saving planet earth, conference proceedings, vols 1 -3*, (SPE 1997), pp. 2227-2230.
24. S. Lawman and H. Liang, "Fourier domain optical coherence tomography for high-precision profilometry", Proc. SPIE 7391, 73910H (2009).
25. A. Podoleanu, I. Charalambous, L. Plesea, A. Dogariu and R. Rosen, “Correction of distortions in optical coherence tomography imaging of the eye”, Phys. Med. Biol., 49, 1277–1294 (2004).
26. S. Ortiz, D. Siedlecki, I. Grulkowski, L. Remon, D. Pascual, M. Wojtkowski and S. Marcos, “Optical distortion correction in Optical Coherence Tomography for quantitative ocular anterior segment by three-dimensional imaging”, Optics Express, 18 (3), 2782-2796 (2010).
27. T. Prykäri, J. Czajkowski, E. Alarousu and R. Myllyla, “Optical Coherence Tomography as an Accurate Inspection and Quality Evaluation Technique in Paper Industry”, Optical Review, 17 (3), 218-222 (2010).
28. J. W. Goodman, *Speckle phenomena in optics, theory and applications* (Roberts & Company, 2007).
29. M. M. Amaral, M. P. Raele, J. P. Caly, R. E. Samad, N. D. Vieira and A. Z. Freitas, Proc. SPIE 7390, 73900Z (2009).
30. G. J. Tearney, M. E. Brezinski, J. F Southern, B. E. Bouma, M. R. Hee and J. G. Fujimoto, “Determination of the refractive index of highly scattering human tissue by optical coherence tomography”, Optics Letters, 20 (21), 2258-2260 (1995).

31. X. Wang, C. Zhang, L. Zhang, L. Xue and J. Tian, “Simultaneous refractive index and thickness measurements of bio tissue by optical coherence tomography”, Journal of Biomedical Optics, 7 (4), pp 628-632 (2002).
32. P. H. Tomlins, P. Wooliams, C. Hart, A. Beaumont and M. Tedaldi, “Optical coherence refractometry”, Optics Letters, 33 (19), 2272-2274 (2008).
33. J. V. Koleske, *Paint and Coating Testing Manual: Fourteenth Edition of the Gardner-Sward Handbook* (ASTM, 1995).

Caption and figure List

1. Fig. 1. (a) A Gaussian fit (solid curve) to the 5 central data points across an air/glass interface. The peak position found by the Gaussian fit is shown by the dashed line; (b) Measured *rms* error of the surface profile of a standard flat surface as a function of the number of frames averaged before fitting.
2. Fig. 2. a) SROCT image of a sinusoidal surface of 1.5 μm peak-to-peak amplitude and 50 μm period; b) Surface profile measured with SROCT (black dots) and a sinusoidal fit to the measurement (solid red curve); c) Surface profile of the same sine surface measured with a Veeco inc. Wyko NT1100 WLI (black dots) and a sinusoidal fit to measurement (solid red curve).
3. Fig. 3. a) SROCT image of a droplet of Regalrez 1094 dissolved in white spirit on a flat microscope slide; b) Positions found from a) including extrapolation of the real position of the microscope slide beneath the droplet; c) Measurement of refractive indices of a drying droplet carried out at 5 minute intervals for 30 minutes, using only data points around the position that the beam is normal to the droplet surface. Error bars of one standard deviation are shown.
4. Fig. 4. (a) Profile of coarse glass substrate measured before (solid black line) and after (red dots) deposition of a varnish solution of Regalrez dissolved in white spirit over half the measured surface profile. The varnish surface is shown by a dashed red curve. The substrate profile below the varnish was recovered by assuming a refractive index of 1.49; (b) Difference between the before and after profiles of the rough glass substrate.
5. Fig. 5. The *rms* difference between the refractive index corrected varnish/substrate interface measurements and the reference measurement before the deposition of the varnish is shown

as a function of the assumed refractive index of the varnish for four independent measurements (solid curves). The dotted vertical line shows the measured refractive index of the varnish from Section 4.1. The horizontal solid line shows the measured speckle error of the substrate surface using the method detailed in Section 3.3. The dashed lines represent the $\pm 1\sigma$ boundaries of this measurement.

6. Fig. 6. Time evolution of the measured surface profile (thick black lines) of a drying AYAT varnish at 10s, 3min 40s, 7min 10s and 14min since the application of the varnish and the profile of the rough glass substrate (thin black line). The corresponding theoretical time evolution of the varnish surface profiles are given in thin green (or gray) curves. (media1)
7. Fig. 7. Power Spectral Densities (PSD) of final surface profile measurements and models of two varnishes applied on similar substrates. The measured PSD of Regalrez varnish surface is shown by the thin solid black line, the modeled PSD is shown by the thin black dashed line and the PSD of vibrational noise is shown by the gray dashed line. The measured PSD of AYAT is shown by the thick red (or black) line and the modeled PSD is shown by the dashed thick magenta (or gray) line. The mean PSD of the two corresponding substrate profiles is shown by the thin light green (or gray) line.
8. Fig. 8. a) The time evolution of the modeled (green or gray lines) and measured (black line) raw *rms* roughness of the surface profile of a drying AYAT varnish coating for the spatial frequencies $>1\text{mm}^{-1}$ (thin line), $<1\text{mm}^{-1}$ (thick line) and the full spatial frequency range (medium thickness line) are shown separately; b) The same as part a) for a drying Regalrez coating; c) The time evolution of the measured (black lines) cross-correlation coefficient between the surface and substrate profile of the drying AYAT varnish for the spatial frequencies $>1\text{mm}^{-1}$ (thin line), $<1\text{mm}^{-1}$ (thick line) are shown separately; the expected $\pm 1\sigma$

bounds of the modeled profiles with vibrational noise are shown in thin green (or gray) lines for the spatial frequencies >1mm^{-1} and in thick green (or gray) lines for frequencies <1mm^{-1}; d) The same as part c) for the drying Regalrez coating; e) Measured (black lines) and modeled (green or gray line) varnish thickness versus time for AYAT; f) Varnish thickness versus time for Regalrez.

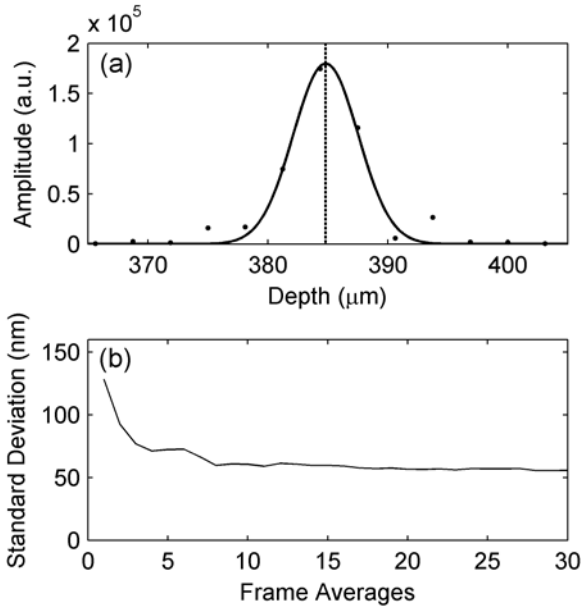
x 10^5
(a)
Amplitude (a.u.)
2
1.5
1
0.5
0
370
380
390
400
Depth (μm)
(b)
Standard Deviation (nm)
150
100
50
0
0
5
10
15
20
25
30
Frame Averages

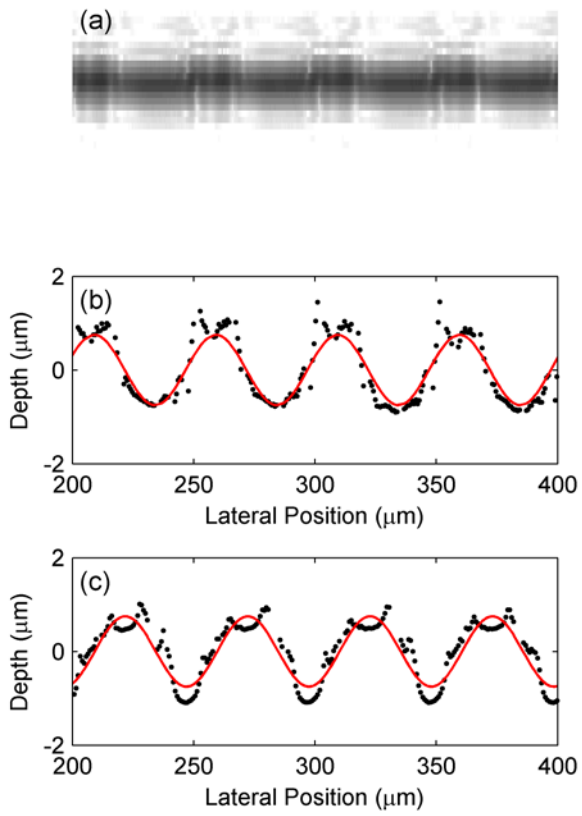
(a)
(b)
Depth (μm)
2
0
-2
200
250
300
350
400
Lateral Position (μm)
(c)
Depth (μm)
2
0
-2
200
250
300
350
400
Lateral Position (μm)

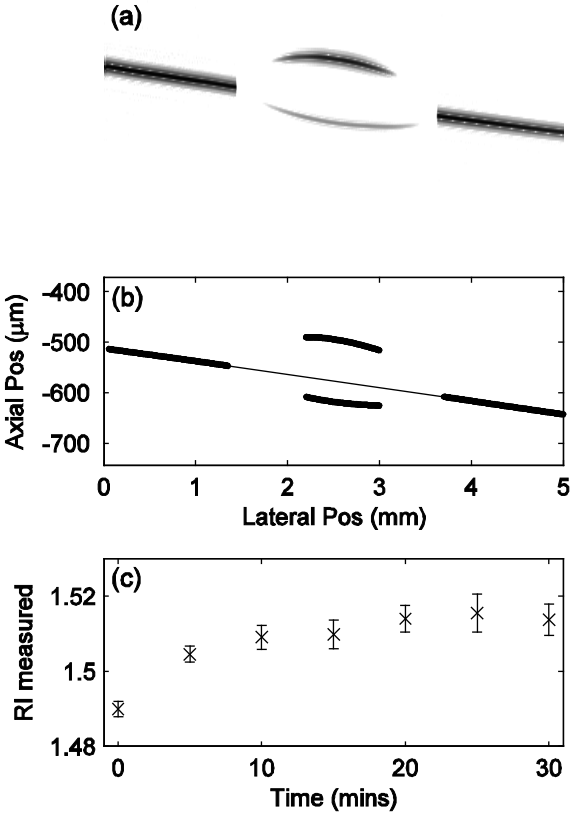
(a)
(b)
Axial Pos (μm)
-400
-500
-600
-700
0
1
2
3
4
5
Lateral Pos (mm)
(c)
RI measured
1.52
1.5
1.48
0
10
20
30
Time (mins)

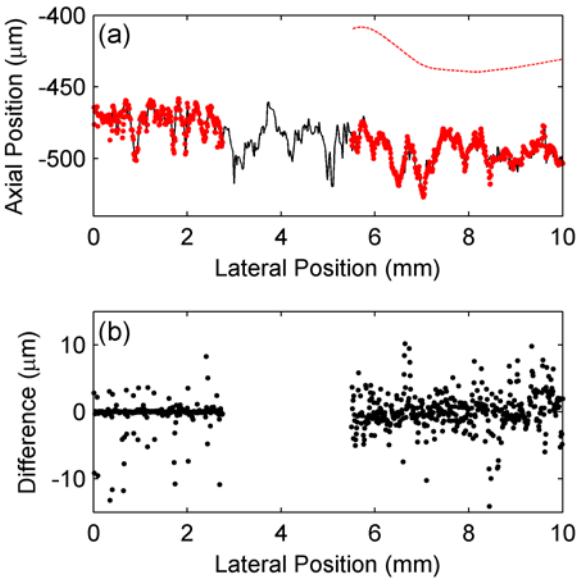
(a)
Axial Position (μm)
-400
-450
-500
0
2
4
6
8
10
Lateral Position (mm)
(b)
Difference (μm)
10
0
-10
0
2
4
6
8
10
Lateral Position (mm)

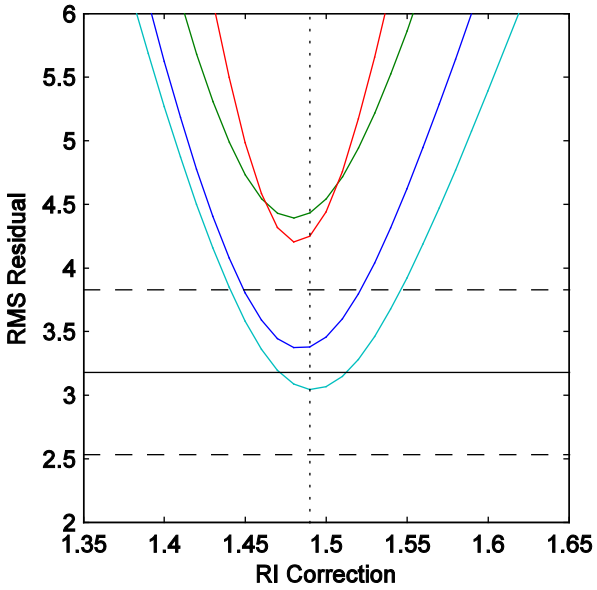
RMS Residual
RI Correction
6
5.5
5
4.5
4
3.5
3
2.5
2
1.35
1.4
1.45
1.5
1.55
1.6
1.65

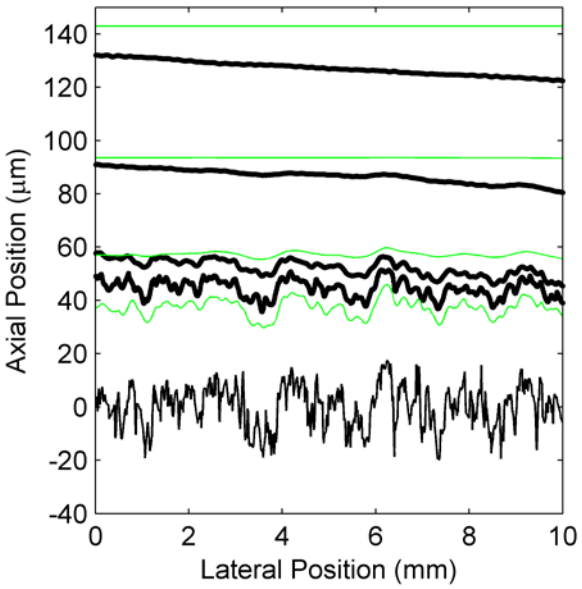
140
120
100
80
60
40
20
0
-20
-40
Axial Position (µm)
0
2
4
6
8
10
Lateral Position (mm)

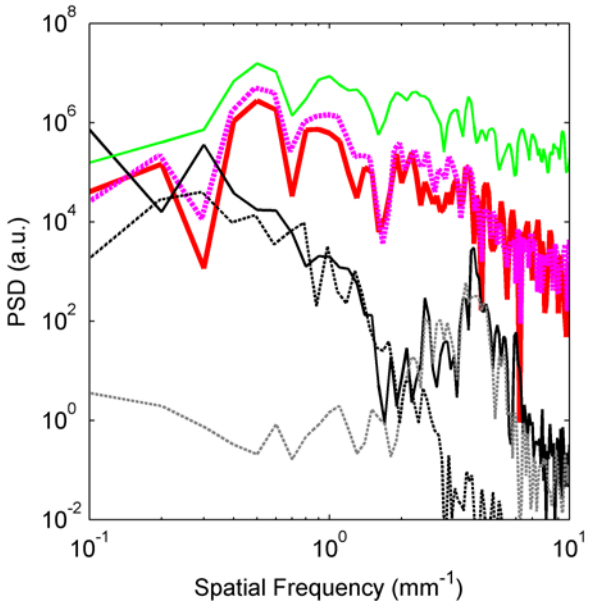
PSD (a.u.)
Spatial Frequency (mm-1)
10^8
10^6
10^4
10^2
10^0
10^-2
10^-1
10^0
10^1

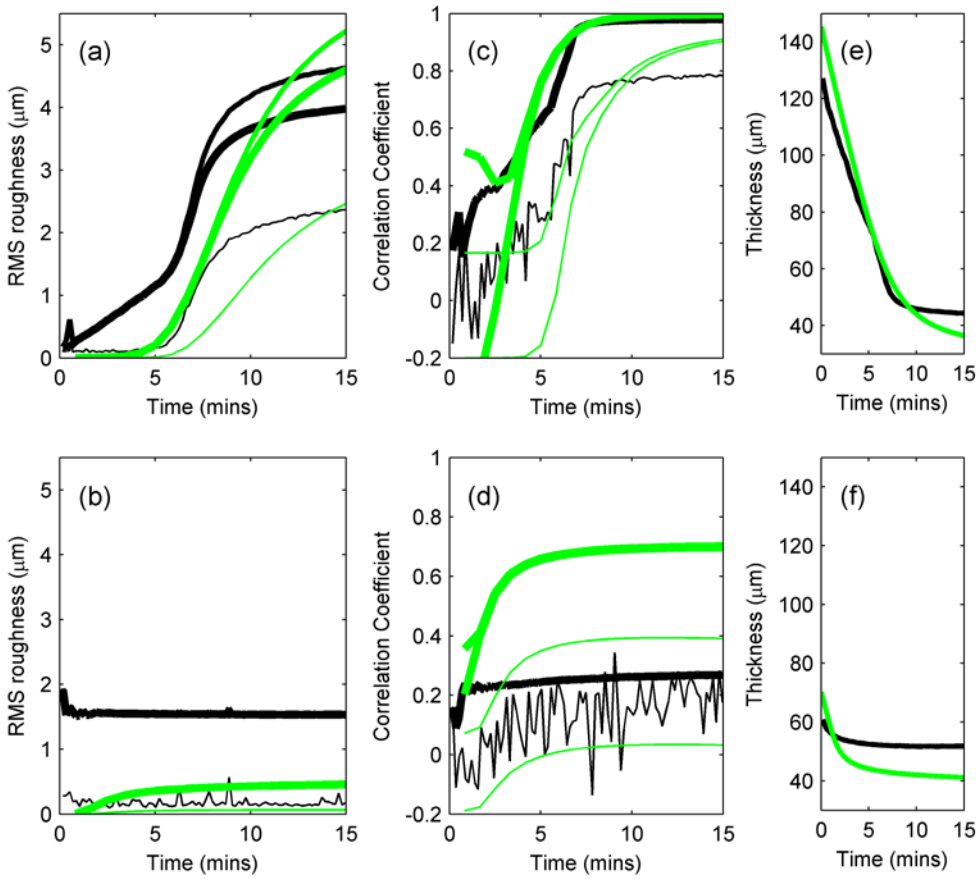
(a)
RMS roughness (μm)
Time (mins)
(c)
Correlation Coefficient
Time (mins)
(e)
Thickness (μm)
Time (mins)
(b)
RMS roughness (μm)
Time (mins)
(d)
Correlation Coefficient
Time (mins)
(f)
Thickness (μm)
Time (mins)